Desalination and Water Treatment
www.deswater.com
doi: 10.1080/19443994.2014.896289

54 (2015) 1694–1707
May

Taylor & Francis
Taylor & Francis Group

Adsorption of lead by activated carbon developed from rice husk

A.M. Youssef[a,*], A.I. Ahmed[a], M.I. Amin[b], U.A. El-Banna[a]

[a]*Faculty of Science, Department of Chemistry, Mansoura University, Mansoura, Egypt, Tel. +20 1005613355; email: amayosef@mans.edu.eg*
[b]*Nuclear Materials Authority, Cairo, Egypt*

Received 4 August 2013; Accepted 25 January 2014

ABSTRACT

Activated carbons were prepared from rice husk for the adsorption of Pb(II) from aqueous solution. The textural properties of the prepared carbons were characterized from the adsorption of nitrogen at 77 K and scanning electron microscopy. Fourier-transform infrared spectroscopy, base and acid neutralization capacities, pH of the active carbon slurry, and pH point of zero charge (pH_{pzc}) were used to characterize the surface oxygen functional groups. The effect of experimental parameters such as pH, initial concentration, contact time, and temperature on the adsorption was investigated. The equilibrium data were analyzed by the Langmuir and Freundlich models, which revealed that Langmuir model was more suitable to describe the lead adsorption than Freundlich model. The adsorption kinetics could be expressed by the pseudo-second-order model where boundary layer diffusion tends to be the rate-limiting step. Solution pH exhibited remarkable impact on the adsorption process and the maximum amount adsorbed was obtained at pH 5. The adsorption capacity of the carbon sample is related to the porosity and the surface chemistry, which are dependent on the method of activation.

Keywords: Adsorption; Rice husk; Activated carbon; Pb(II)

1. Introduction

The removal of heavy metals from water is important in terms of protecting public health and environment owing to their accumulation in living tissue throughout the food chain as non-biodegradable pollutants [1,2]. Lead is recognized as a long-standing environment contaminant. It can be found in wastewater generated by various industries such as acid battery, ceramic, glass manufacturing, metal plating, electroplating, mining, and smelters [3]. Acute lead poisoning in human beings causes severe damage to the kidney, liver, brain, nervous system, a rise in blood pressure, miscarriage, and abortions [4,5]. There are various techniques for reducing the toxicity of heavy metals, including chemical precipitation, adsorption, electrolysis, ion exchange, and membrane separation [6]. Adsorption onto activated carbon was found to be a promising technique as it enables the removal of trace amount of lead from solution [7]. Fortunately, activated carbons can be prepared from renewable biomass materials including apricot stone [8], hazelnut husks, coconut shells, peanut shells, and rubber wood sawdust [9,10]. Rice husk (RH) accounts for about 20% of the total weight of rice plants. The processing and transformation of RHs into activated carbon with good adsorption properties would

*Corresponding author.

alleviate problems of disposal and management of these waste by-products and produce value-added products from RHs for wastewater treatment. Most of the activated carbons are produced by thermal procedures (physical) or chemical routes [11,12].

This article reports the preparation of low-cost ACs from RH by sodium hydroxide and steam activation. The textural properties and the chemistry of the surface of the carbons and their roles towards the removal of Pb(II) from aqueous solution by static batch experiments were investigated. In addition, the effect of experimental parameters such as solution pH, initial concentration, contact time, and temperature was studied. Furthermore, equilibrium, kinetic and thermodynamic studies on the adsorption of Pb(II) onto the activated carbon were also carried out for the design of adsorption process.

2. Experimental

2.1. Materials

RH from the rice mill of El-Mansoura city (Egypt) was used as raw material. RH was first washed with distilled water to remove dust and other adhering impurities and then dried at 383 K for 48 h. Finally, the dried product was ground and sieved to different particle sizes. Studies were focused on size fraction 0.3–0.5 mm. Lead nitrate was supplied by BDH. A stock solution of lead (1,000 mg/L) was prepared by dissolving the required amount of $Pb(NO_3)_2$ in double-distilled water. The stock solution was diluted with distilled water to obtain the desired concentration. Other chemicals used were of analytical grade. Before use, all the glass wares were washed with nitric acid and then washed with doubly distilled water.

2.2. Preparation of activated carbons (adsorbents)

2.2.1. Preparation of non-activated carbons HC and LC

Sample HC was prepared as following: 100 mL of 13 M sulfuric acid was added to the RH, and the mixture was heated to 448–453 K for 20 min with occasional stirring. The resulting black mixture was allowed to cool and then filtered using a Buchner funnel under vacuum. The black spent sulfuric acid was filtered off and the carbonized material was washed several times with distilled water and was stored [13].

Carbonization product LC was prepared by carbonization of dried RH pre-leached with HF. Leaching was made at room temperature using 25% analytical grade hydrofluoric acid. The acid solution volume-to-mass ratio was 2.5:1. Dried HF-leached RH was calcined separately in the absence of air in batch process using stainless steel reactor at a rate of 10 K/min from room temperature up to 773 K and soaking at this final temperature for 3 h.

2.2.2. Preparation of physically activated carbon (SLC)

Steam activated carbon (SLC) was obtained by gasifying a portion of LC carbon with a mixture of nitrogen and steam at 1,173 K to burn off = 29 wt.%. Sample LC was contained in a stainless steel tube positioned vertically in a tubular muffle furnace. The entering gas mixture was passed through the "LC" bed, which was supported upon a fine chromel screen. The flow rate was sufficient to keep the sample "Jiggling." This was achieved by passing nitrogen as a diluent through the sample during steam run [14].

2.2.3. Preparation of chemically activated carbon

An activated sample NLC was prepared by soaking LC in the presence of substantial weight of analytical grade NaOH, dissolved in the least amount of water for 48 h (carbon: solid NaOH = 1:3 W/W). The paste was then dried. After that, the dried product was calcined at a rate of 10 K/min to the final temperature of 1,123 K, which was maintained for 3 h. After cooling, the resulting mixture was washed with hot distilled water until pH 6.5 to eliminate activating agent residues and other inorganic species formed during the process. The carbon obtained was dried at 383 K for use in adsorption and analytical investigations [15].

2.2.4. Oxidation of the activated carbons

Samples Ox-NLC and Ox-SLC were prepared by heating SLC and NLC with concentrated nitric acid (10 mL/g carbon) to almost dryness at 363 K followed by washing and drying [16].

2.3. Characterization of prepared activated carbon

2.3.1. Low-temperature adsorption of nitrogen

The textural properties (surface area and porosity) of the activated carbons were investigated using a volumetric apparatus of conventional type. The adsorbent was degassed at 473 K under reduced pressure of 10^{-5} torr for 8 h prior to adsorption measurements. The surface area, S_{BET}, was determined from isotherms using the Brunauer–Emmett–Teller equation [17]. The total pore volume V_T (mL/g) was also

calculated from the volume of nitrogen adsorbed near saturation, i.e. at $P/P^\circ = 0.95$. Another textural parameter, i.e. the mean pore radius $\bar{r}$ (nm) was calculated from the relationship:

$$\bar{r} = \frac{2V_T \times 10^3}{S_{\mathrm{BET}}} \quad (1)$$

Additional information was obtained by comparison with standard adsorption data on a reference non-porous carbon. Thus, volume of N_2 adsorbed at specific relative pressures (V_a) is plotted against the corresponding standard reduced value (α_s) at same relative pressure (α_s-plot). Standard data given by Selles-Perez and Martin-Martinez were utilized [18]. An estimate for the total surface area S^α was determined from slope of the line connecting the early points to the origin, and the non-microporous surface area S_n^α from the slope of the line connecting the high pressure data (beyond $\alpha_s = 1.0$). Extrapolation of the latter linear section to meet the V_a-axis represents the volume within micropores (V_m^α). The volume of nitrogen adsorbed at relative pressure = 0.1 may be taken as a measure of the micropore volume V_{mic}.

2.3.2. Scanning electron microscopy

Scanning electron microscopy (SEM): Micrographs of SLC and NLC were obtained using scanning electron microscope (SEM; JEOL, model 6400). Prior to the analysis, the samples were dried at 110°C for 4 h. A thin layer of gold was coated on the samples for charge dissipation.

2.3.3. Chemistry of the carbon surfaces

2.3.3.1. Surface functional group determination. Fourier-transform infrared (FT-IR) spectroscopy: FT-IR spectra were recorded between 4,000 and 400 cm^{-1} using a Mattson 5000 FT-IR spectrometer. Disks were prepared by first mixing 1 mg dried carbon sample with 500 mg of KBr (Merck for spectroscopy) in an agate mortar and then pressing the resulting mixture at 5 tonne/cm^2 for 5 min and 10 tonne/cm^2 for 5 min under vacuum.

2.3.3.2. Selective neutralization analysis. Acid and basic functional groups on the AC surface were determined by the method proposed by Boehm [19]. Solution of $NaHCO_3$ (0.05 N), Na_2CO_3 (0.05 N), NaOH (0.05 and 0.15 N), and HCl (0.05 N) were prepared using CO_2-free distilled water. A 25 mL volume of these solutions was added to vials containing 0.25 g of AC. These samples were shaken until equilibrium. When equilibrium was reached, the carbon was separated from solution by filtration. The excess of base or acid was determined by back titration using (HCl 0.05 and 0.15 N) and NaOH (0.05 N) solutions.

2.3.3.3. Determination of pH of the slurry. About 0.5 g of carbon sample was shaken with 25 mL CO2-free distilled water and then, the pH of filtrate was measured.

2.3.3.4. Determination of PH_{PZC}. Initially, 50 mL of NaCL was placed in several closed Erlenmeyer flasks. The PH within each flask was adjusted to a value between 2 and 12 by adding either HCl (0.1 M) or NaOH (0.1 M). Then, 0.15 g was added to each flask, the flasks were agitated for 48 h, and the final PH was then measured. The PH_{PZC} is defined by the point where the curve PH_{final} vs. $PH_{initial}$ crosses the line $pH_{final} = pH_{initial}$ [20].

2.4. Adsorption studies

The adsorption experiments were carried out by contacting precisely weighted sample of carbon with 50 mL of Pb(II) in the sealed 100 mL Erlenmeyer flasks. The flasks were then shaken at 150 rpm in a constant temperature shaker at pre-selected temperature for 24 h. The effect of contact time (0–300 min), concentration (50–500 mg/L), and solution pH (2–6) was studied at 298 K. After equilibrium, the solutions were filtered, and the concentration of Pb(ll) ions was determined using an atomic absorption spectrophotometer (JBT 932 EA SP).

3. Results and discussions

3.1. Textural properties

Fig. 1 shows the nitrogen adsorption–desorption isotherms at 77 K of SLC, HC, NLC, Ox-NLC, and Ox-SLC. The isotherms show the characteristics of type I and type II of the BDDT classification [21]. The isotherms exhibit steep initial part and well-developed knee bend at $P/P^\circ = 0.1$–0.2. The narrow closed hysteresis loop exhibited by the sorbent investigated may be taken as an evidence of capillary condensation and the existence of both micro- and mesopores. The α_s-plots (Fig. 2) are corresponding to type α1-b and α1-a classification, indicating the developed porosity in the carbons. Detailed characteristics of the porosity of these carbons were summarized in Table 1.

Inspection of Table 1 shows the following: (1) Carbonization by concentrated sulfuric acid is associated with the observed increase of S_{BET}, V_T, and $\bar{r}$

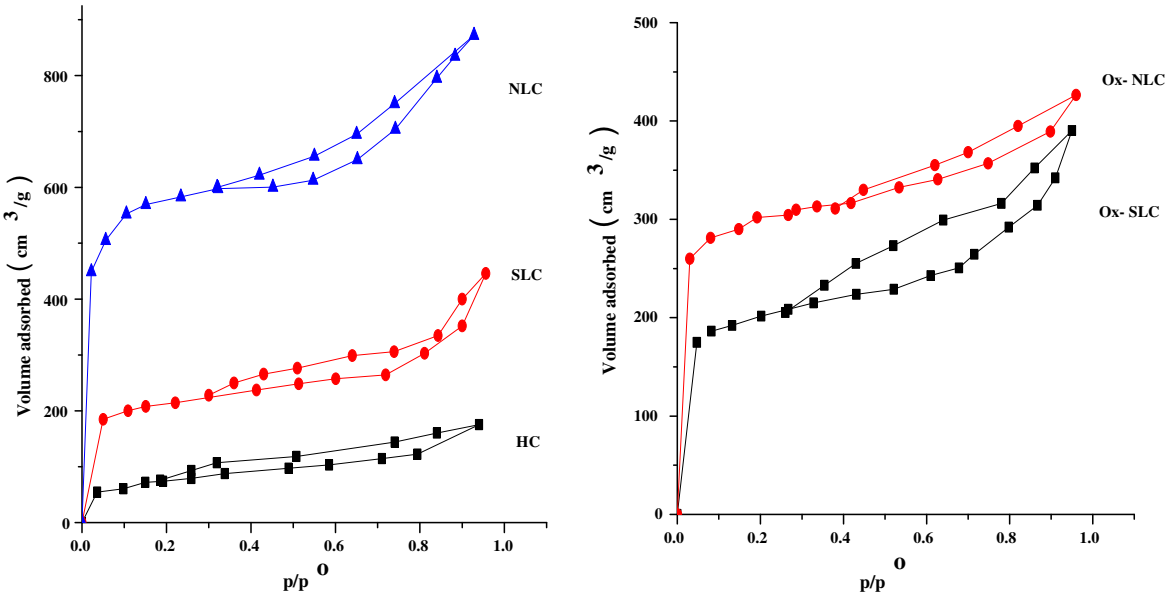

Fig. 1. Nitrogen adsorption–desorption isotherm at 77 K for different carbons samples.

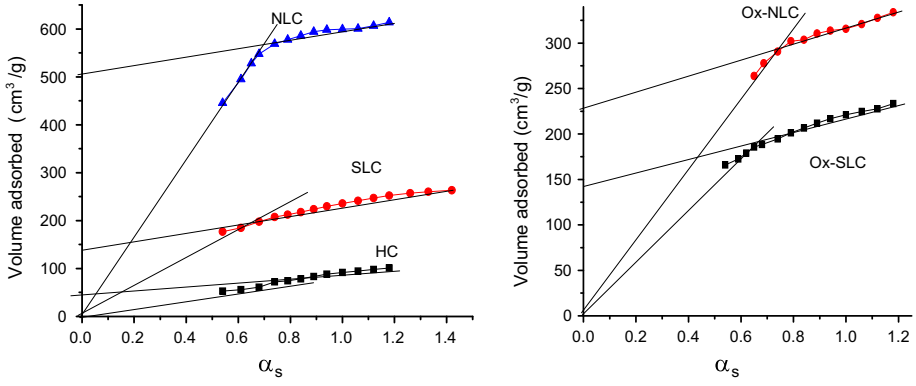

Fig. 2. α_s-plots for nitrogen adsorption– desorption isotherm at 77 K on different carbons samples.

Table 1
Textural properties of the investigated carbons as determined from nitrogen adsorption at 77 K

Sample	S_{BET} (m^2/g)	S^{α} (m^2/g)	S_m^{α} (m^2/g)	S_n^{α} (m^2/g)	V_m^{α} (mL/g)	V_m^{α} (mL/g)	V_{mic} (mL/g)
HC	245.7	263.2	114.4	148.5	0.20	0.07	*0.093*
SLC	770.6	830.1	701.5	128.5	0.30	0.30	*0.310*
NLC	2,254.2	2,275.3	1,808.1	467.5	0.69	0.69	*0.856*
Ox-SLC	610.1	614.3	446.2	168.2	0.23	0.36	*0.289*
Ox-NLC	1,038.6	1,108.1	876.7	231.4	0.27	0.38	*0.437*

Note: The significance of the italic values represent the volume of micropores.

because of a drastic destruction of the structure of precursor, dehydration, oxidation, erosion of narrow pores, and dissolving a large fraction of inorganic content. (2) Steam activation to a burn off = 29% enhances creation of new pores and burning of redeposited carbons inside the pores leading to increase in the surface area and in the total pore volume compared with LC. (3) Activation of LC with considerable amounts of NaOH at 1,023 K resulted in tremendous increase in the surface area and total pore volume because NaOH may react with the carbon which resulted in a loss of carbon according to the following equation [22]:

$$4NaOH + C \rightarrow Na_2CO_3 + Na_2O + 2H_2 \quad (2)$$

(4) The reduction in surface area and pore volume after oxidation with nitric acid may be related to several factors such as: pore entrance blockage by oxygenated surface functional groups and large molecules of residual humic-type compounds, electrostatic repulsion of surface probe molecule (nitrogen), and erosion of carbon by nitric acid.

3.2. SEM

The SEM images (Fig. 3) show the morphology of the samples. The morphologies of activated carbons show irregular shapes. The surface of the activated carbon developed erratic cracking and enhanced roughness and flaking. Many large pores were clearly found on the surface of the activated carbon. The well-developed pores had led to the large surface area and porous structure of the activated carbon.

3.3. Chemistry of the carbon surface

3.3.1. FT-IR analysis

Fig. 4 shows FT-IR spectra for carbon samples (SLC, HC, NLC, Ox-NLC, and Ox-SLC). All the carbon samples show wide band at about (3,250–3,425 cm^{-1}) due to O–H stretching mode of hexagonal group and adsorbed water. The shoulders observed at (2,850–2,950 cm^{-1}) due to aliphatic (C–H) and appear for all carbon samples [23]. The bands near 1,600 cm^{-1} are due to C=C stretching vibration in aromatic ring and are observed for SLC and HC. Very small peak near 1,700 cm^{-1} due to (C=O) stretching vibrations of ketones, aldehydes, lactones, or carboxyl groups is observed in sample (SLC) [24]. The weak intensity of this peak indicates that prepared activated carbon contains small amount of carboxyl group. The broad absorption within the range (1,300–1,000 cm^{-1}) can be ascribed to various C–O bonds such as those in ethers, phenols, and esters [25]. The HNO_3-treated carbon shows a significantly different trend in the FT-IR spectra. Firstly, the appearance of a sharp absorption peak at 1,670–1,730 cm^{-1} indicates the abundant introduction of carboxyl–carbonate structures. The bands at (1,715–1,730 cm^{-1}) for Ox-SLC and Ox-NLC are due to stretching vibration of carboxyl groups on the edges of layer plane [26].

3.3.2. pH slurry, pH (PZC), and Boehm titration

The pH of SLC and NLC slurries was 6.06 and 6.99, respectively. The pH of the slurries for HC, Ox-SLC, and Ox-NLC is 2.2, 2.4, and 2.8 which indicates

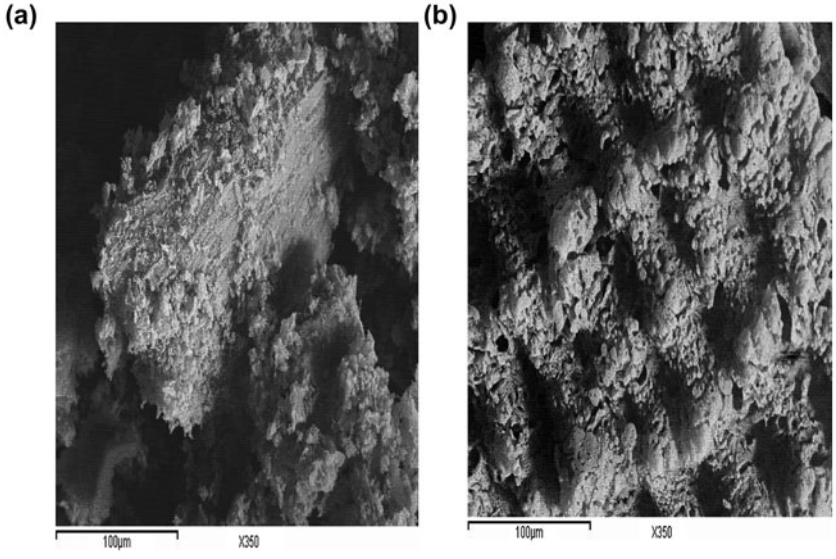

Fig. 3. SEM for activated carbons: (a) SLC and (b) NLC.

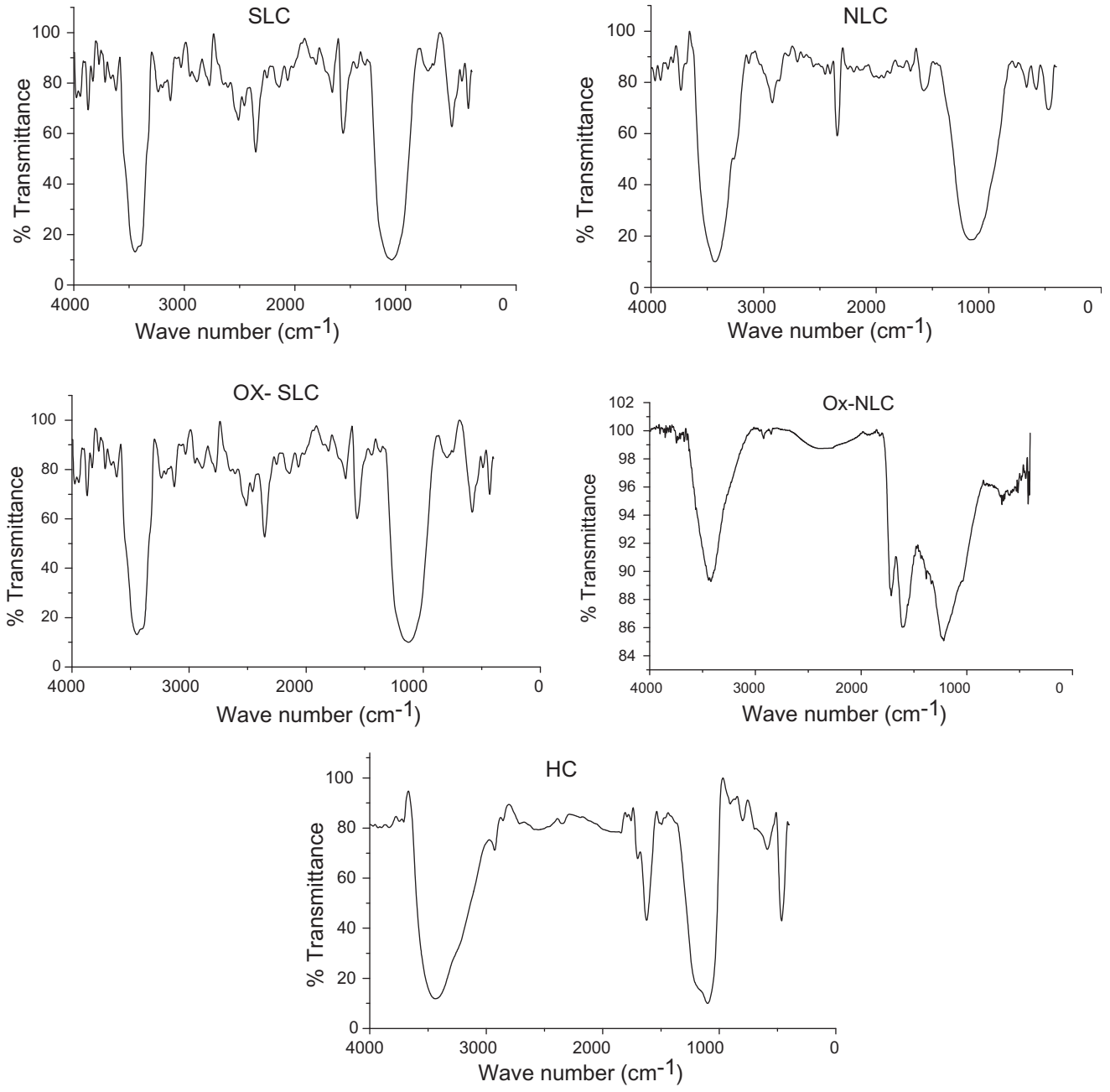

Fig. 4. FT-IR spectra of different carbon samples.

the domination of Bronsted acidic groups on their surfaces. The pH_{pzc} is defined as the pH where the net surface charge is zero. pH_{pzc} can be also considered as the pH value below which the surface of the carbon particles in solution is, on average, positively charged, the converse being true for $pH > pH_{pzc}$. Oxidation of SlC and NLC was brought about a drastic decrease in the pH of their slurries as well as of their pH_{pzc} due to the pronounced increase in the concentration of acidic groups on their surface.

The chemistry of the surface of the AC is better determined from their base neutralization capacities (meq/g). $NaHCO_3$ neutralizes carboxylic groups, whereas these neutralized by Na_2CO_3 but not by $NaHCO_3$ were believed to be lactones. The weakly acidic groups neutralized by NaOH but not by Na_2CO_3 were postulated as phenols. Neutralization with 0.15 N NaOH was assumed to determine all the acidic functional groups on the surface including Carbonyl groups.

The functional groups on the surfaces of the ACs are listed in Table 2 expressed as (meq/g).

Table 2 reveals that the increase in the total oxygenated group is generally associated with a decrease in the value of pH_{pzc}. HC sample measured high neutralization capacity, i.e. 6.77 meq/g. This can be attributed to the severe conditions used in the preparation of this sample, which led to carbonaceous materials loaded with oxygenated groups on the surface. NLC showed low acidic character due to the high activation temperature, which may result in the decomposition of acidic groups. Oxidation with concentrated nitric acid creates new carboxylic groups.

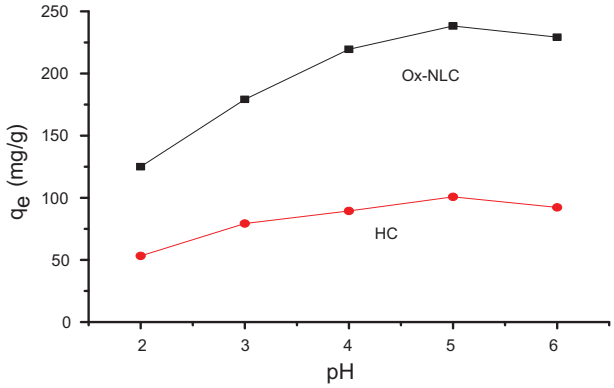

Fig. 5. Effect of pH on adsorption of lead ions Pb(II) on HC and OxNLC.

3.4. Lead adsorption

3.4.1. Effect of pH

The equilibrium amount of lead adsorbed at pH values between 2 and 6 was calculated from the equation:

$$q_e = \frac{(C_0 - C_e)V}{M} \quad (3)$$

where C_0 and C_e are the initial and equilibrium concentrations (mg/L), respectively, V is the volume of adsorption solution (L), and M is the mass of carbon sample (g). The amount adsorbed by ox-NLC increased from 125 at (pH 2) to 238.26 at (pH 5) and for sample HC from 53.24 at (pH 2) to 100.704 at (pH 5) (Fig. 5). At low pH, the surface of the adsorbent was surrounded by hydronium ions that compete with metal ions, preventing the metal ions from approaching the binding sites on the adsorbent. When the pH level increases, the covered H_3O^+ leaves the carbon surface and makes the active sites available to Pb(II). The final equilibrium pH of the reaction mixture was found to be (1.8, 2.7, 3.7, 4.5, and 5.4) for HC and (1.6, 2.5, 3.4, 4.4, and 5.3) for OX-NLC where the initial pH was (2, 3, 4, 5, and 6) indicating that an ion-exchange mechanism between (H^+ and Pb(II)) may be included in the adsorption of Pb(II). In addition, the negative charge on the surface of carbon increases because pH value is higher than pH_{pzc} and the oxygen-containing functional groups became deprotonated with the increase in pH so the electrostatic attraction between AC and Pb(II) was enhanced, increasing the amount of Pb(II) adsorption according to equation:

$$2(\text{S-COH}) + \text{M}^2 \leftrightarrow (\text{S-CO})_2\ \text{M} + 2\text{H}^+$$

At pH 5.0, the adsorption capacity of (HC and Ox-NLC) almost reaches the maximum value. Because the speciation diagram of lead shows that at pH > 6.0 species such as $[Pb(OH)]^+$, $[Pb_3(OH)_4]^+$, and $[Pb(OH)_2]$ will be produced [27]. In order to guarantee to truly examine the adsorption property of carbon samples as

Table 2
Functional groups (meq/g), surface pH, and pH_{pzc} of the prepared carbons

Carbon	Carboxylc (meq/g)	Lactonic (meq/g)	Phenolic (meq/g)	Carbonyl (meq/g)	Total acidic	Total basic	Surface pH	pH_{pzc}
SLC	0.33	0.07	0.36	1.15	1.91	1.10	6.06	7.39
NLC	0.07	0.24	0.07	0.07	0.45	0.31	6.99	6.56
Ox-SLC	0.66	0.09	0.38	1.17	2.30	0.17	2.42	3.63
Ox-NLC	0.97	0.17	0.17	1.21	2.52	0.09	2.85	3.23
HC	2.52	1.28	0.74	2.23	6.77	0	2.26	3.04

well as to avoid precipitation of Pb(II) ions, all the following experiments were conducted at pH 5.0.

3.4.2. The effect of contact time

The amount of lead adsorbed at time t, q_t (mg/g), was calculated from equation:

$$q_e = \frac{(C_0 - C_t)V}{M} \tag{4}$$

where C_t (mg/L) is the concentration of the metal adsorbed at time t. As seen in Fig. 6, the adsorption of Pb(II) ions increased sharply during the first 30 min and attained equilibrium within 2 h. The fast adsorption at the initial stage may be due to the higher driving force leading to fast transfer of metal ions to the surface of adsorbent particles and the availability of the active sites on the adsorbent. To ensure that sufficient contact time was obtained, further adsorption experiments were carried out for 8 h.

3.4.3. Adsorption kinetic

To evaluate adsorption kinetics, two common models were applied to the experimental data obtained at adsorption processes. These are pseudo-first order and pseudo-second order. The differential form of the pseudo-first-order model of adsorption can be expressed [28] as:

$$\frac{dq_t}{dt} = k_1(q_e - q_t) \tag{5}$$

where q_e and q_t (mg/g) are the amounts of lead adsorbed at equilibrium and at time t, respectively, and k is the equilibrium constant (min^{-1}). Integration of Eq. (2) and by applying the initial conditions $q_t = 0$ at $t = 0$:

$$\log(q_e - q_t) = \log q_e - \frac{k_1}{2.303}t \tag{6}$$

The differential form of the pseudo-second-order reaction equation may be written as [29]:

$$dq_t/d_t = k_2(q_e - q_t)^2 \tag{7}$$

where K_2 is the pseudo-second rate constant (mg/g min). After integration considering the boundary conditions, the linearized form of this model is given as:

$$\frac{t}{q_t} = \frac{1}{k_2 q_{e^2}} + \frac{1}{q_e}t \tag{8}$$

A comparison of the different kinetic models for the adsorption of Pb(II) onto (HC and Ox-NLC) is illustrated in Fig. 7. It can be seen that the pseudo-first-order kinetic curves do not give a good fit to the experimental kinetic data. This disagreement can also be confirmed by low R^2 values. On the contrary, the results presented an ideal fit to the pseudo-second-order model with the extremely high R^2 (0.9998–0.9999). A good agreement can further be supported by the similar values of the calculated and experimental values of q_e. The values of the parameters and the correlation coefficient obtained by two kinetic models are listed in Table 3.

3.4.4. Mechanism of adsorption

The mechanism of adsorption is usually demonstrated by three steps [30]. 1—Film diffusion, which involves the movement of adsorbate molecules from the bulk of the solution towards the external surface of the adsorbent. 2—Transfer of ions from the surface to the intraparticular active sites (particle diffusion). 3—Adsorption of ions by the active sites of adsorbent. Because the third step is a very rapid process, it does not belong to the rate-controlling steps. Therefore, the rate-controlling steps mainly depend on either film diffusion or particle diffusion. The intraparticle diffusion model was first proposed by Weber and Morris [31] who concluded that the uptake was proportional to the square root of the contact time during the course of adsorption, i.e.

$$q_t = K_d t^{0.5} + C \tag{9}$$

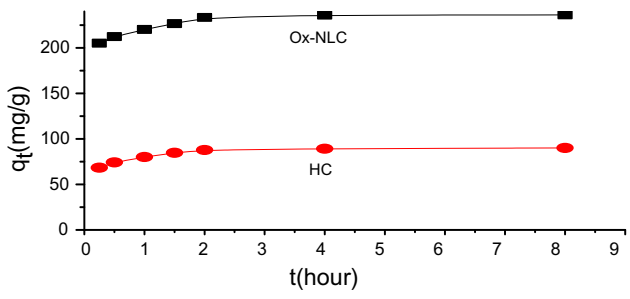

Fig. 6. Kinetic for adsorption of Pb(II) onto HC and Ox-NLC.

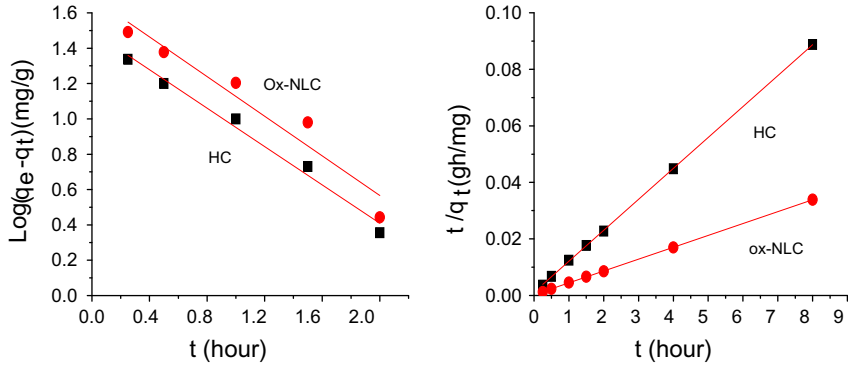

Fig. 7. Pseudo-first order and pseudo-second order for adsorption of Pb(II) by HC and Ox-NLC.

Table 3
First- and second-order kinetic parameters for adsorption of lead on HC and Ox-NLC

Sample	$q_{e,\ exp}$ (mg/g)	Pseudo-first-order kinetic model			Pseudo-second-order-kinetic-model		
		q_{e1} (mg/g)	K_1 (1/h)	R^2	q_{e2} (mg/g)	K_2 (g/mgh)	R^2
Hc	90.1	31.2	1.2	0.981	91.7	0.069	0.999
Ox-NLC	236.2	48.7	1.3	0.916	238.1	0.073	0.999

where K_d is the rate constant of the intraparticle diffusion [mg/gh$^{0.5}$]. The value of K_d is obtained from the slope of the straight line, whereas C is the intercept. The value of C is a measure of the thickness of the boundary layer. The larger the intercept, the greater is the boundary layer effect. The parameters K_d, C, and R^2 are listed in Table 4. According to this model, the dual nature of the curves may be attributed to the difference of the adsorption extents in the initial and final stages. The first steep portion stands for the external surface adsorption, and the second portion raises gradually with the intraparticle diffusion. If the intraparticle diffusion is the rate-limiting step, the plot of q_t vs. $t^{1/2}$ should be linear and pass through the origin. None of the intraparticle diffusion plots passed through the origin which revealed that the intraparticle diffusion was part of the adsorption but was not the only rate-controlling step and refers to the effect of film diffusion (boundary layer diffusion).

In order to predict the actual slow step involved, the kinetic data were further analyzed using the Boyd kinetic model to distinguish between film diffusion and particle diffusion. Boyd kinetic equation [32] was applied, which is represented as:

$$F(t) = 1 - \frac{6}{\pi^2}\sum_{n=1}^{\infty}\frac{1}{n^2}\exp(-n^2Bt) \tag{10}$$

where f *is* the fractional attainment of equilibrium at different times (t), and $B(t)$ is a mathematical function of F.

$$f = \frac{q_t}{q_e} \tag{11}$$

where q_t and q_e is the amount adsorbed at time (t) and equilibrium, respectively.

Table 4
Intraparticle diffusion and Boyd plot parameters for adsorption of lead onto investigated carbons

Samples	Intraparticle diffusion			Boyd plot	
	K_d (mg/gh$^{0.5}$)	C (mg/g)	R^2	Intercept	R^2
HC	1.57	85.79	0.902	0.88	0.925
Ox-NLC	1.84	231.20	0.85	1.00	0.982

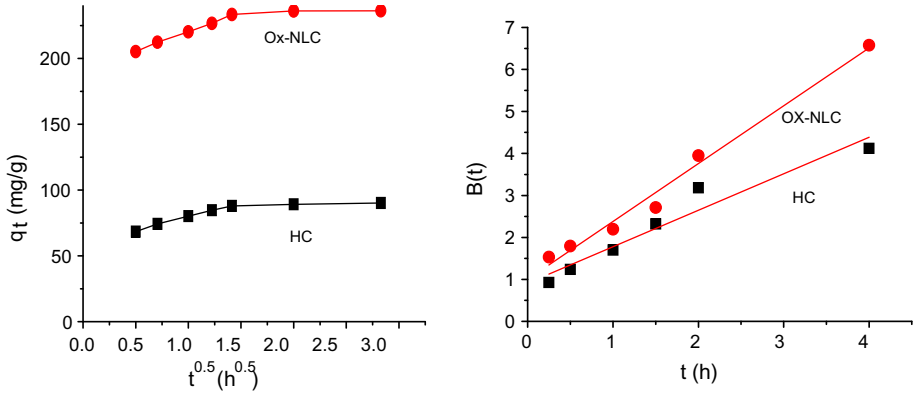

Fig. 8. Intraparticle diffusion and Boyd plots for different carbon samples.

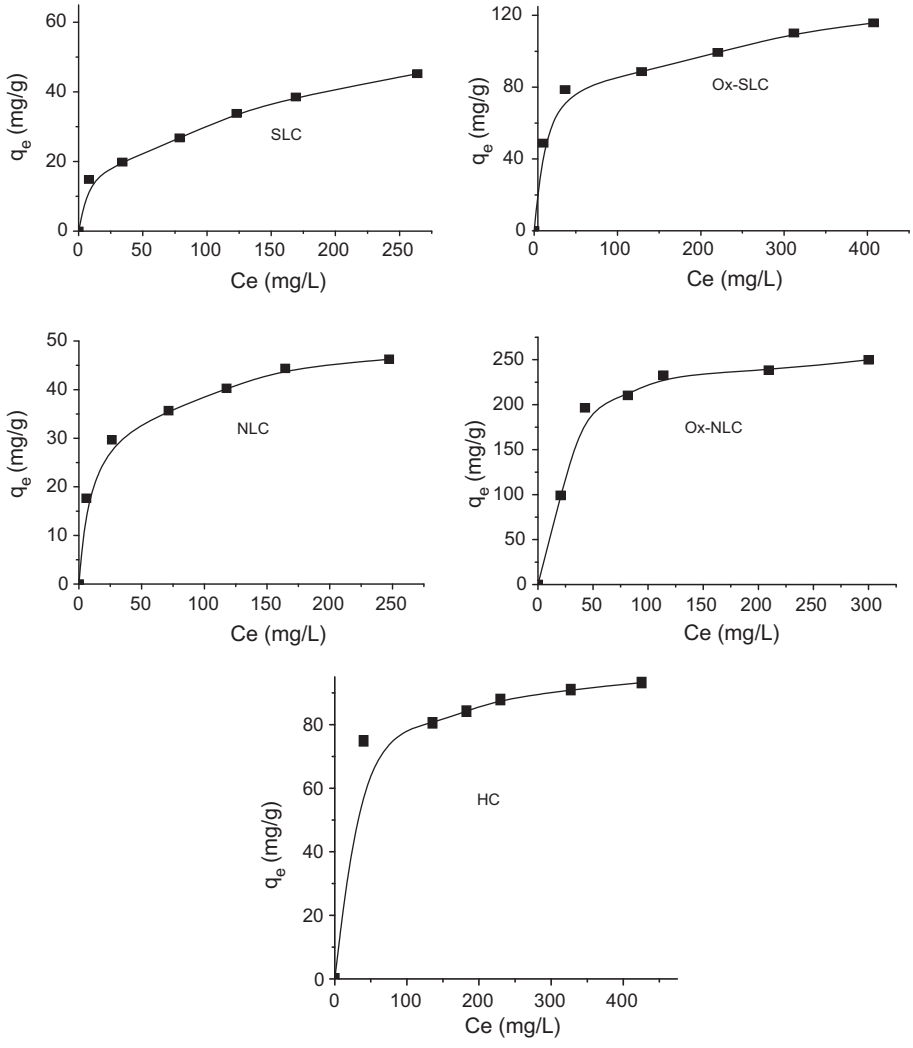

Fig. 9. Equilibrium adsorption isotherm of lead on different carbon samples.

Reichenberg [33] managed to obtain the following approximations:

$$B(t) = -0.4977 - \ln(1 - F) \text{ for } F \text{ values} > 0.85 \quad (12)$$

and for

$$F \text{ values} < 0.85,\ B(t) = \left(\sqrt{\pi} - \sqrt{\pi - \left(\frac{\pi^2 F(t)}{3}\right)}\right)^2 \quad (13)$$

The plot of $B(t)$ against time t can be employed to test the linearity of the experimental values. If the plots are linear and pass through origin, then the slowest (rate controlling) step in the adsorption process is the internal diffusion, and vice versa. Fig. 8 shows that the plots are linear but do not pass though the origin suggesting that the adsorption process is controlled by film diffusion.

3.5. Equilibrium adsorption isotherm

The isotherm data were obtained by plotting amount of lead adsorbed on the solid (mg/g) against the remaining concentration of lead in the solution (mg/L). The equilibrium isotherms describe how the adsorbent interacts with the adsorbate. Equilibrium adsorption isotherms are illustrated in Fig. 9. The correlation of experimental results to adsorption model can help to understand the mechanisms of adsorption. Two isotherm models, namely, Langmuir and Freundlich were employed to describe the adsorption of Lead.

The Langmuir adsorption isotherm [34] assumes that adsorption occurs at specific homogenous sites within the adsorbent and makes the estimation of adsorption capacities under various conditions a simple task. The linear form of Langmuir isotherm can be represented as:

$$\frac{C_e}{q_e} = \frac{1}{bq_{mon}} + \frac{1}{q_{mon}} C_e \quad (14)$$

where q_e is the equilibrium concentration of lead on the adsorbent (mg/g), C_e the equilibrium concentration in the solution (mg/dm^3), q_m is the maximum adsorption capacity (mg/g), and b (L/mg) is known as the Langmuir constant related to the heat of adsorption.

A straight line of slope $= \frac{1}{q_m}$ and intercept of $\frac{1}{bq_m}$ is obtained when C_e/q_e is plotted against C_e. One of the essential characteristics of the Langmuir isotherm

Table 5
Langmuir and Freundlich constants for adsorption of Pb(II) by carbon samples

Sample	Langmuir parameters			Freundlich parameters		
	q_{max} (mg/g)	b (L/mg)	R^2	K_f (mg/g)	n	R^2
SLC	51.1	0.021	0.970	6.88	3.04	0.962
Ox-SLC	119.9	0.032	0.989	30.87	4.54	0.938
NLC	49.2	0.054	0.994	11.82	3.90	0.974
Ox-NLC	261.7	0.053	0.998	124.461	8.13	0.921
HC	100.7	0.029	0.999	51.77	10.46	0.947

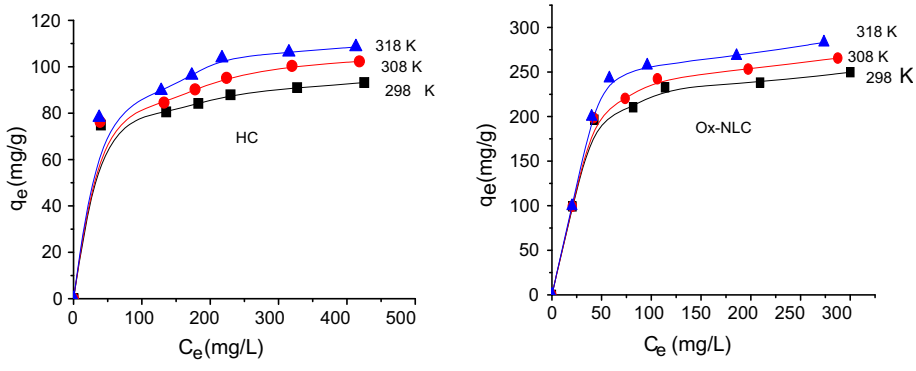

Fig. 10. Adsorption isotherm for HC and Ox-NLC at different temperatures.

Table 6
Langmuir and Freundlich constants for adsorption of lead by (HC and Ox-NLC) at different temperatures

		298 K			308 K			318 K		
	Sample	q_{max} (mg/g)	b (L/mg)	R^2	q_{max} (mg/g)	b (L/mg)	R^2	q_{max} (mg/g)	b (L/mg)	R^2
Langmuir constants	HC	100.7	0.029	0.999	108.2	0.035	0.995	115.6	0.0371	0.996
	Ox-NLC	261.2	0.053	0.998	279.3	0.058	0.999	298.5	0.059	0.998
		25 K			35 K			45 K		
		K_f (mg/g)	n	R^2	K_f (mg/g)	n	R^2	K_f (mg/g)	n	R^2
Freundlich constants	HC	42.9	7.8	0.947	46.4	7.6	0.954	49.4	6.896	0.958
	Ox-NLC	124.4	8.1	0.921	130.3	8	0.897	167. 0	10.86	0.967

can be expressed by a separation factor, R_L; which is defined as:

$$R_L = \frac{1}{1 + bC_0} \tag{15}$$

where C_0 is the highest initial solute concentration. The R_L value implies whether the adsorption is unfavorable ($R_L > 1$), linear ($R_L = 1$), favorable ($0 < R_L < 1$), or irreversible ($R_L = 0$). It is observed that all the R_L values obtained were between 0 and 1, showing that the adsorption of lead on the activated carbon was favorable. The R_L values decrease with the increase in initial lead concentration, indicating that the adsorption was more favorable at higher lead concentration.

The Freundlich equation [35] can be applied to non-ideal sorption on heterogeneous surfaces as well as multi-layer sorption and is expressed by the following equation:

$$\ln q_e = \ln K_f + \frac{1}{n} \ln C_e \tag{16}$$

where K_f and n are Freundlich constants related to adsorption capacity and adsorption intensity, respectively. Isotherm parameters were calculated and summarized in Table 5. As shown in the table, the correlation coefficients for the linear Langmuir regression fits are larger than that for the Freundlich plot so the Langmuir model could describe well the adsorption isotherms of Pb(II) uptake from aqueous solution throughout the whole range of concentrations.

Table 5 shows that pronounced Pb(II) uptake was associated with tremendous increase in the surface acidity of the activated carbon and a noticeable decrease in its surface area so it can be concluded that the surface acidity, ion exchange, electrostatic attraction, and coordination with COOH functional groups enhance Pb(II) adsorption compared with the role of the textural parameters.

3.6. Adsorption thermodynamics

In order to determine the thermodynamic parameters, the sorption studies were carried out at different temperatures for two samples (HC and Ox-NLC). Fig. 10 shows the effect of temperature on adsorption of lead at three different temperatures on HC and Ox-NLC. Table 6 shows the increase in uptake of Pb^{2+} with temperature which can be ascribed to the increase in the adsorption rate of

Table 7
Thermodynamic parameters for adsorption of lead onto HC and Ox-NLC at different temperatures

Sample	ΔS° (J/mole K)	ΔH° (kJ/mole)	ΔG° (kJ/mole)		
			298 K	308 K	318 K
HC	+94.1	+5.1	−5.359	−22.76	−23.64
Ox-NLC	+32.9	+9.5	−23.01	−24.01	−24.91

lead ions and the change in size of pores, indicating that the adsorption is an endothermic process.

The change in standard free energy, (ΔG°), of adsorption was calculated from the following equation:

$$\Delta G^\circ = -RT \ln b \tag{17}$$

where R is gas constant, T is temperature in K, and b is Langmuir constant (L/mole). Standard enthalpy (ΔH°) and entropy (ΔS°) of adsorption could be estimated from van't Hoff equation:

$$\ln b = \frac{-\Delta H^\circ}{RT} + \frac{\Delta S^\circ}{R} \tag{18}$$

The slope and intercept of van't Hoff plot are equal to $\frac{-\Delta H^\circ}{RT}$ and $\frac{\Delta S^\circ}{R}$, respectively. The values of ΔG°, ΔH°, and ΔS° are shown in Table 7. The negative values of ΔG° indicate the spontaneous nature of adsorption process. The positive value of enthalpy change indicates that the adsorption is endothermic in nature. This is also observed from the increase in adsorption capacity with temperature. ΔS values are all positive indicating that the adsorbed lead is more free on the adsorption sites of activated carbon than in aqueous medium.

4. Conclusions

Activated carbon with high surface area can be prepared form RH, a residue of the agricultural activity. The activated carbon modified with nitric acid shows low surface area and higher acidity compared to other carbon samples except HC. Lead adsorption was dramatically enhanced after the carbon was oxidized, which indicates that adsorption is mainly dependant on coordination with surface functional groups. The optimum pH range for adsorption of lead was five. The maximum adsorption capacity for sample Ox-NLC was 263 mg/g. The adsorption of lead followed pseudo-second-order kinetics, and the adsorption is controlled by boundary layer effect. The adsorption was found to be spontaneous and endothermic.

References

[1] R. Gündoğan, B. Acemioğlu, M.H. Alma, Copper(II) adsorption from aqueous solution by herbaceous peat, J. Colloid Interface Sci. 269 (2004) 303–309.
[2] A. Sari, M. Tuzen, D. Citak, M. Soylak, Adsorption characteristics of Cu(II) and Pb(II) onto expanded perlite from aqueous solution, J. Hazard. Mater. 148 (2007) 387–394.
[3] M. Momčilović, M. Purenović, A. Bojić, A. Zarubica, M. Ranđelović, Removal of lead(II) ions from aqueous solutions by adsorption onto pine cone activated carbon, Desalination 276 (2011) 53–59.
[4] W. Shi, H. Shao, H. Li, M. Shao, S. Du, Progress in the remediation of hazardous heavy metal-polluted soils by natural zeolite, J. Hazard. Mater. 170 (2009) 1–6.
[5] M.E. Argun, S. Dursun, M. Karatas, M. Gürü, Activation of pine cone using Fenton oxidation for Cd(II) and Pb(II) removal, Bioresour. Technol. 99 (2008) 8691–8698.
[6] A.H. Sulaymon, B.A. Abid, J.A. Al-Najar, Removal of lead copper chromium and cobalt ions onto granular activated carbon in batch and fixed-bed adsorbers, Chem. Eng. J. 155 (2009) 647–653.
[7] K.G. Sreejalekshmi, K.A. Krishnan, T.S. Anirudhan, Adsorption of Pb (II) and Pb (II)-citric acid on sawdust activated carbon: Kinetic and equilibrium isotherm studies, J. Hazard. Mater. 161 (2009) 1506–1513.
[8] A.M. Youssef, N.R.E. Radwan, I. Abdel-Gawad, G.A.A. Singer, Textural properties of activated carbons from apricot stones, Colloids Surf. A 252 (2005) 143–151.
[9] M. Soleimani, T. Kaghazchi, Adsorption of gold ions from industrial wastewater using activated carbon derived from hard shell of apricot stones—An agricultural waste, Bioresour. Technol. 99 (2008) 5374–5383.
[10] M. Sekar, V. Sakthi, S. Rengaraj, Kinetics and equilibrium adsorption study of lead(II) onto activated carbon prepared from coconut shell, J. Colloid Interface Sci. 279 (2004) 307–313.
[11] K. Sun, J.C. Jiang, Preparation and characterization of activated carbon from rubber-seed shell by physical activation with steam, Biomass Bioenerg. 34 (2010) 539–544.
[12] T.H. Liou, Development of mesoporous structure and high adsorption capacity of biomass-based activated carbon by phosphoric acid and zinc chloride activation, Chem. Eng. J. 158 (2010) 129–142.

[13] E.I. El-Shafey, Removal of Zn (II) and Hg (II) from aqueous solution on a carbonaceous sorbent chemically prepared from rice husk, J. Hazard. Mater. 175 (2010) 319–327.
[14] M.N. Alaya, M.A. Hourieh, A.M. Youssef, Adsorption properties of activated carbons prepared from olive stones by chemical and physical activation, Adsorpt. Sci. Technol. 18 (2000) 27–42.
[15] M.A.L. Rodenas, D.L. Castello, D.C. Amoros, A.L. Solano, Preparation of activated carbon from Spanish anthracite II, activation by NaOH, Carbon 39 (2001) 751–759.
[16] J. Jaramillo, P.M. Álvarez, V.G. Serrano, Oxidation of activated carbon by dry and wet methods, Fuel Process. Technol. 91 (2010) 1768–1775.
[17] S. Brunauer, P.H. Emmett, E. Teller, Adsorption of gases in multimolecular layers, J. Am. Chem. Soc. 60 (1938) 309–319.
[18] M.J.S. Perez, J.M. Martinez, Application of α and n plots to N_2 adsorption isotherms of activated carbons, J. Chem. Soc., Faraday Trans. 87 (1991) 1237–1243.
[19] H.P. Boehm, Surface oxides on carbon and their analysis: A critical assessment, Carbon 40 (2002) 145–149.
[20] J.J.M. Órfão, A.I.M. Silva, J.C.V. Pereira, S.A. Barata, I.M. Fonseca, P.C.C. Faria, M.F.R. Pereira, Adsorption of a reactive dye on chemically modified activated carbons—Influence of pH, J. Colloid Interface Sci. 296 (2006) 480–489.
[21] E. Tütem, R. Apak, C.F. Ünal, Adsorptive removal of chlorophenols from water by bituminous shale, Water Res. 32 (1998) 2315–2324.
[22] Y. Guo, S. Yang, K. Yu, J. Zhao, Z. Wang, H. Xu, The preparation and mechanism studies of rice husk based porous carbon, Mater. Chem. Phys. 74 (2002) 320–323.
[23] L.J. Kennedy, J.J. Vijaya, G. Sekaran, Electrical conductivity study of porous carbon composite derived from rice husk, Mater. Chem. Phys. 91 (2005) 471–476.
[24] L.J. Kennedy, J.J. Vijaya, G. Sekaran, Effect of two-stage process on the preparation and characterization of porous carbon composite from rice husk by phosphoric acid activation, Ind. Eng. Chem. Res. 43 (2004) 1832–1838.
[25] Y. Guo, D.A. Rockstraw, Physical and chemical properties of carbons synthesized from xylan, cellulose, and Kraft lignin by H_3PO_4 activation, Carbon 44 (2006) 1464–1475.
[26] S. Biniak, M. Pakuła, G.S. Szymański, A. Świątkowski, Effect of activated carbon surface oxygen- and/or nitrogen-containing groups on adsorption of copper (II) Ions from aqueous solution, Langmuir 15 (1999) 6117–6122.
[27] L. Wang, J. Zhang, R. Zhao, Y. Li, C. Li, C. Zhang, Adsorption of Pb(II) on activated carbon prepared from *Polygonum orientale* Linn: Kinetics, isotherms, pH, and ionic strength studies, Bioresour. Technol. 101 (2010) 5808–5814.
[28] S. Langergren, B.K. Svenska, Zur theorie der sogenannten adsorption geloester stoffe, Veternskapsakad Handlingar. 24 (1898) 1–39.
[29] Y.S. Ho, C.C. Chiang, Sorption studies of acid dyes by mixed sorbents, Adsorption 7 (2001) 139–147.
[30] J.-W. Kim, M.-H. Sohn, D.-S. Kim, S.-M. Sohn, Y.-S. Kwon, Production of granular activated carbon from waste walnut shell and its adsorption characteristics for Cu^{2+} ion, J. Hazard. Mater. 85 (2001) 301–315.
[31] W.J. Weber, J.C. Morris, Kinetics of adsorption on carbon solution, J. Sanit. Eng. Div. ASCE 89 (1963) 31–59.
[32] G.E. Boyd, A.W. Adamson, L.S. Myers Jr., The exchange adsorption of ions from aqueous solutions by organic zeolites, II: Kinetics, J. Am. Chem. Soc. 69 (1947) 2836–2848.
[33] D. Reichenberg, Properties of ion-exchange resins in relation to their structure. III. Kinetics of exchange, J. Am. Chem. Soc. 75 (1953) 589–597.
[34] I. Langmuir, The adsorption of gases on plane surfaces of glass, mica and platinum, J. Am. Chem. Soc. 40 (1918) 1361–1403.
[35] H.M.F. Freundlich, Over the adsorption in solution, J. Phys. Chem. 57 (1906) 385–470.